

# Discriminant Analysis and Secondary-Beam Charge Recognition

J. Lukasik<sup>a,i</sup>, P. Adrich<sup>a</sup>, T. Aumann<sup>a</sup>, C.O. Bacri<sup>c</sup>, T. Barczyk<sup>d</sup>, R. Bassini<sup>e</sup>,  
 S. Bianchin<sup>a</sup>, C. Boiano<sup>e</sup>, A.S. Botvina<sup>a,f</sup>, A. Boudard<sup>g</sup>, J. Brzychczyk<sup>d</sup>, A. Chbihi<sup>h</sup>,  
 J. Cibor<sup>i</sup>, B. Czech<sup>i</sup>, J.-É. Ducret<sup>g</sup>, H. Emling<sup>a</sup>, J. Frankland<sup>h</sup>, M. Hellström<sup>a</sup>,  
 D. Henzlova<sup>a</sup>, G. Immè<sup>b</sup>, I. Iori<sup>e</sup>, H. Johansson<sup>a</sup>, K. Kezzar<sup>a</sup>, A. Lafriakh<sup>c</sup>, A. Le Fèvre<sup>a</sup>,  
 E. Le Gentil<sup>g</sup>, Y. Leifels<sup>a</sup>, J. Lühning<sup>a</sup>, W.G. Lynch<sup>j</sup>, U. Lynen<sup>a</sup>, Z. Majka<sup>d</sup>, M. Mocko<sup>j</sup>,  
 W.F.J. Müller<sup>a</sup>, A. Mykulyak<sup>k</sup>, M. De Napoli<sup>b</sup>, H. Orth<sup>a</sup>, A.N. Otte<sup>a</sup>, R. Palit<sup>a</sup>,  
 P. Pawłowski<sup>i</sup>, A. Pullia<sup>e</sup>, G. Raciti<sup>b</sup>, E. Rapisarda<sup>b</sup>, H. Sann<sup>a,1</sup>, C. Schwarz<sup>a</sup>, C. Sfiinti<sup>a</sup>,  
 H. Simon<sup>a</sup>, K. Sümmerer<sup>a</sup>, W. Trautmann<sup>a</sup>, M.B. Tsang<sup>j</sup>, G. Verde<sup>j</sup>, C. Volant<sup>g</sup>,  
 M. Wallace<sup>j</sup>, H. Weick<sup>a</sup>, J. Wiechula<sup>a</sup>, A. Wieloch<sup>d</sup> and B. Zwiegliński<sup>k</sup>

<sup>a</sup>*Gesellschaft für Schwerionenforschung mbH, D-64291 Darmstadt, Germany*

<sup>b</sup>*Dipartimento di Fisica e Astronomia dell'Università and INFN-LNS and Sez. CT, I-95123 Catania, Italy*

<sup>c</sup>*Institut de Physique Nucléaire, IN2P3-CNRS et Université, F-91406 Orsay, France*

<sup>d</sup>*M. Smoluchowski Institute of Physics, Jagiellonian University, PL-30059 Kraków, Poland*

<sup>e</sup>*Istituto di Scienze Fisiche, Università degli Studi and INFN, I-20133 Milano, Italy*

<sup>f</sup>*Institute of Nuclear Research, Russian Academy of Science, Ru-117312 Moscow, Russia*

<sup>g</sup>*DAPNIA/SPhN, CEA/Saclay, F-91191 Gif-sur-Yvette, France*

<sup>h</sup>*GANIL, CEA et IN2P3-CNRS, F-14076 Caen, France*

<sup>i</sup>*IFJ-PAN, PL-31342 Kraków, Poland*

<sup>j</sup>*Department of Physics and Astronomy and NSCL, MSU, East Lansing, MI 48824, USA*

<sup>k</sup>*A. Soltan Institute for Nuclear Studies, PL-00681 Warsaw, Poland*

---

## Abstract

The discriminant-analysis method has been applied to optimize the exotic-beam charge recognition in a projectile fragmentation experiment. The experiment was carried out at the GSI using the fragment separator (FRS) to produce and select the relativistic secondary beams, and the ALADIN setup to measure their fragmentation products following collisions with Sn target nuclei. The beams of neutron poor isotopes around  $^{124}\text{La}$  and  $^{107}\text{Sn}$  were selected to study the isospin dependence of the limiting temperature of heavy nuclei by comparing with results for stable  $^{124}\text{Sn}$  projectiles. A dedicated detector to measure the projectile charge upstream of the reaction target was not used, and alternative methods had to be developed. The presented method, based on the multivariate discriminant analysis, allowed to increase the efficacy of charge recognition up to about 90%, which was about 20% more than achieved with the simple scalar methods.

*Key words:* Statistical methods, discriminant analysis, radioactive beams, projectile fragmentation

*PACS:* 02.50.Sk, 25.70.Mn

---

## 1. Introduction

The ALADIN experiment S254, conducted in 2003 at the SIS heavy-ion synchrotron at GSI

---

*Email address:* j.lukasik@gsi.de (J. Lukasik).

<sup>1</sup> deceased

Darmstadt, was designed to study isotopic effects in projectile fragmentation at relativistic energies. Besides stable  $^{124}\text{Sn}$  beams, neutron-poor secondary Sn and La beams were used in order to extend the range of isotopic compositions beyond that available with stable beams alone. The secondary beams were produced at the fragment separator FRS [1] by the fragmentation of primary  $^{142}\text{Nd}$  projectiles with energies of about 900 MeV per nucleon in a thick beryllium target. The FRS was set to select  $^{124}\text{La}$  and, in a second part of the experiment, also  $^{107}\text{Sn}$  secondary projectiles of 600 MeV per nucleon which were then delivered to the experiment.

In order to reach the necessary beam intensity of about 1000 particles/s with the smallest possible mass-to-charge ratio  $A/Z$ , it was found necessary to reduce the thickness of the degrader at the dispersive focus (S2) of the FRS (see Fig. 1) that is normally used for the selection of isotopically pure secondary beams. As a result, the beams arriving at the reaction target contained a distribution of neighbouring isotopes together with the nominal  $^{124}\text{La}$  or  $^{107}\text{Sn}$ . The  $A/Z$  of each projectile is known from the measured position at the dispersive focus (S2) and from its flight time over the more than 80 m beam line between the plastic scintillator at S8 (FRS exit) and the start detector at the entrance of the ALADIN setup (Figs. 1 and 2). The atomic number  $Z$ , however, could only be measured for non-interacting projectiles with the MUSIC IV tracking detector placed downstream of the ALADIN dipole magnet.

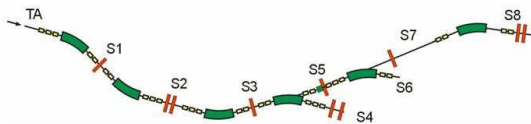


Fig. 1. Schematic FRS beam line setup. The primary beam from SIS enters the production target area (TA) from the left. S1-S8 - focal planes. S2 - dispersive focus, S8 - secondary beam exit to Cave B and C (after <http://www-w2k.gsi.de/frs-setup>).

In order to minimize the upstream material, only two thin plastic detectors were mounted near the reaction target (Fig. 2): the start detector, for measuring the arrival time of each projectile, and the position detector, for measuring the projectile position in the plane perpendicular to the beam direction. No detector with the resolution necessary to resolve individual  $Z$ 's in the  $Z \approx 50$  region was placed there. It will be shown in the following that,

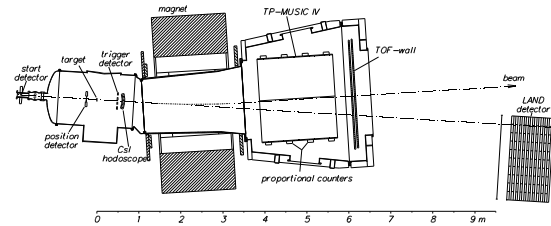


Fig. 2. S254 setup in Cave B. The secondary beams from the FRS enter the experimental area from the left (see Ref. [2]).

with a discriminant method, the atomic number  $Z$  of interacting projectiles can, nevertheless, be reconstructed with high resolution by combining the amplitude and time information available from all the upstream detectors (S2, S8, start and position).

## 2. Discriminant analysis

Discriminant analysis (DA) is a statistical method for predicting a class membership for a set of vectors of observations based on a set of observations for which the classes are known (a training set). For the training set, DA searches for a transform – a projection onto a lower-dimensional vector space – such that the ratio of the between-class distance to the within-class distance is maximized, thus assuring maximum discrimination. The optimal reference frame onto which the projection is made, is found by solving the generalized eigenvalue problem for the scatter matrices (see e.g. [3–5] and their references) defined for the training set. For a training set composed of  $K$  classes, each  $n_k$  in number, the total,  $\mathcal{S}_T$ , and the within-class,  $\mathcal{S}_W$ , scatter matrices can be defined using the notion of covariance matrix:

$$\mathcal{S}_T = N\mathcal{C}_T,$$

$$\mathcal{S}_W = \sum_{k=1}^K n_k \mathcal{C}_W^k,$$

and the between-class scatter matrix,  $\mathcal{S}_B$ , can be simply expressed as a difference<sup>2</sup>:

$$\mathcal{S}_B = \mathcal{S}_T - \mathcal{S}_W.$$

Here,  $N = \sum_{k=1}^K n_k$ , is the total number of vectors of observations in the training set and  $\mathcal{C}_T$  and  $\mathcal{C}_W^k$  are the covariance matrices, built of the vectors of observations, for the total set and for each individual class,  $k$ , respectively.

<sup>2</sup> See e.g. [3, 4] for a strict definition

The optimal reference frame is found as a sub-set of eigenvectors  $\vec{v}$  solving the generalized eigenvalue problem:

$$\mathcal{S}_B \vec{v} = \lambda \mathcal{S}_T \vec{v}. \quad (1)$$

An important property of DA is its dimensionality reduction. Since the rank of  $\mathcal{S}_B$  cannot be greater than  $(K-1)$  and the rank of a product cannot exceed the ranks of the components, the optimal frame, in which the classes are best separated, is spanned by at most  $(K-1)$  eigenvectors. This means, for example, that for a 3-class training set considered here (see next section) and 189 dimensional vectors of observations, the problem gets reduced after DA to 2 dimensions, such that the structure of the original high-dimensional space is preserved in the low-dimensional space. The problem can then easily be handled with *e.g.* 2 dimensional histograms. It should be noted that, to avoid the singularity problem, the initial dimensionality should not exceed the number of vectors of observations [4].

DA has a broad range of applications: from its pioneering application in plant taxonomy [6], through applications *e.g.* in image recognition, marketing, diagnosis in medicine, to those in nuclear physics [5,7]. We found it also very well suited for recognizing the charge of secondary beams from the GSI fragment separator used as projectiles in the S254 experiment [2]. In order to minimize the background from the reactions up-stream, the ionization chambers, normally used in secondary-beam experiments to determine the  $Z$  of the beam, were not used in S254. The charge of the beam entering Cave B could only be measured precisely for the projectiles which did not interact with the target, using the MUSIC IV tracking chamber positioned down-stream of the target (see Fig. 2). In order not to overload the data stream with these non-interacting-beam events, only a selected fraction of them has been allowed to trigger (after scaling down) and these events were used as the training set.

### 3. Results and discussion

From realistic simulations of the beam transport, it was found that the most promising observable to determine the up-stream charge is the position of the beam at the target. During the experiment this was measured with the position-sensitive plastic scintillator detector required for the tracking of projectile fragments and positioned just in front of the target

(see Fig. 2). Optionally, some other simple observables could be considered as beam charge sensitive as, *e.g.*, the energy loss in the plastic detectors up-stream (S2, S8, start or position, see Fig. 2) or the  $A/Z$  variation with the  $Z$  of the beam.

All these beam charge correlated scalar observables, together with the “reference” energy loss in the MUSIC chamber and the final multidimensional-DA projection, have been tested for their charge discrimination power. Figure 3 presents distributions of these observables for the training set of secondary beams of  $Z = 57 \pm 1$ , for a selected  $A/Z$  interval [2.183, 2.203] containing the  $^{125}\text{La}$  isotope, and plotted in the range of  $\pm 4$  standard deviations from the mean of the total spectrum. The three histograms in each panel represent three classes of the beam charge ( $Z = 56$  - dotted histogram, 57 - solid and 58 - dashed) and are labeled according to the charge identification derived from the energy loss in the MUSIC chamber.

The top panel of Fig. 3 shows a “reference” charge distribution of secondary beams as measured by the MUSIC chamber for non-interacting projectiles from the same run. This observable served to label the classes of the training set. It is unavailable for projectiles that underwent fragmentation in the target but, from the experimental point of view, of interest for analyses requiring a precise knowledge of the atomic number  $Z$  besides the known  $A/Z$ .

The three middle panels present the corresponding “charge distributions” obtained by measuring the horizontal position of the beam at the target (corresponding to the dispersive coordinate of the FRS), the energy loss in the position detector, and the high resolution  $A/Z$ .

The bottom panel of the figure shows the same three classes of charge plotted as projections on the eigenvector corresponding to the largest eigenvalue, obtained using the DA technique with 189 dimensional input vectors of observations (see Fig. 4 for a corresponding 2-dimensional original projection). The components of these input vectors of observations (features) contain the information from all the up-stream detectors, *i.e.* the times and amplitudes from the S2 and S8 FRS scintillators [1], the start detector and from the position detector in front of the target. All together 18 raw signals which were combined in addition into pair products to maximize the DA efficiency (see *e.g.* [7]), finally resulting in 189 features.

The figure demonstrates that the high charge resolution obtained with the MUSIC chamber is dif-

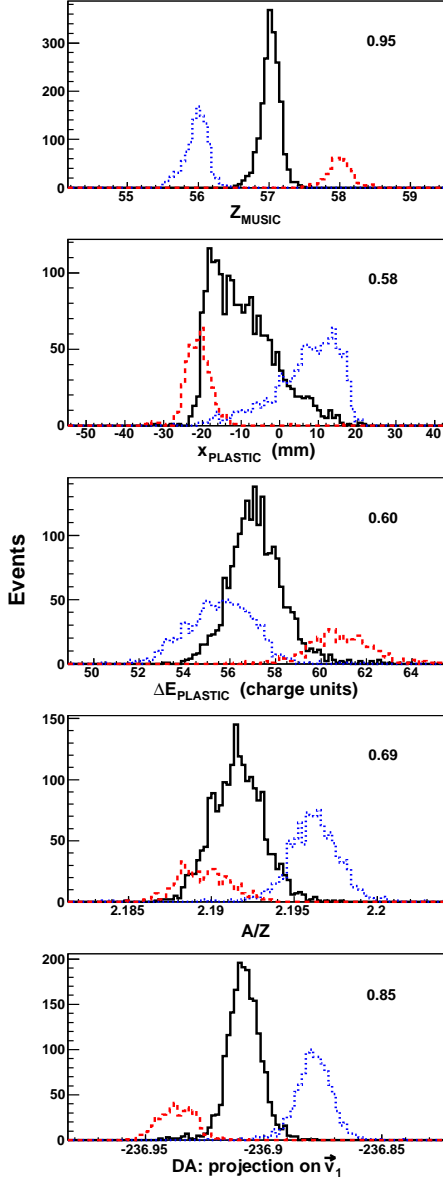


Fig. 3. (Color online) Charge distributions for  $Z = 57 \pm 1$  beams of the training set obtained from the (from top to bottom) energy loss in the MUSIC chamber, horizontal position of the beam at the target, energy loss  $\Delta E_{\text{PLASTIC}}$  in the position detector, high resolution  $A/Z$  and the DA with 189 dimensional input vectors of observations projected on the eigenvector corresponding to the larger eigenvalue (bottom, see Fig. 4). The numbers (top-right) specify the discrimination power [7] of the observable. The spectra are plotted in the range of  $\pm 4$  standard deviations of the total. The solid ( $Z = 57$ ), dotted ( $Z = 56$ ) and dashed ( $Z = 58$ ) histograms represent three classes of the beam charge labeled according to the energy loss in the MUSIC chamber.

difficult to be achieved or surpassed with other simple observables. However, combining all the possible

pieces of information in an optimal way using the DA method allows to improve the resolution and to come much closer to the reference.

One way to quantify the resolution of an observable is to determine its discrimination power. It is defined as [7]:

$$\lambda = \frac{\mathcal{S}_B}{\mathcal{S}_T}$$

for 1-dimensional vectors of observations (scalar observables) and as an appropriate eigenvalue of (1) for the multidimensional case.  $\lambda \in [0, 1]$  and is equal to zero when the classes have the same mean values and equal to one when, for all classes, all the vectors of observations of a given class are equal but distinct from those of the other classes. Discrimination powers for the tested observables have been specified in the top-right corner of each panel of Fig. 3.

The discrimination among classes becomes even better since in actual discrimination procedures we consider at least three classes at a time and thus deal with at least two-dimensional projections. Fig. 4 shows the original 2-dimensional scatter plot for the three classes of charge considered here which was the base for the one-dimensional projection presented in the bottom panel of Fig. 3. The distribution results from the projection of the original 189-dimensional vectors of observations on the two main eigenvectors obtained with the DA technique.

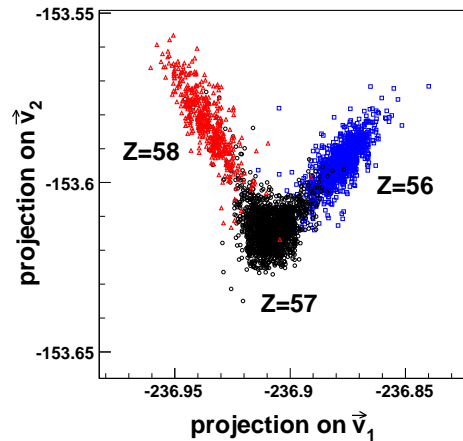


Fig. 4. (Color online) Projections of the original 189-dimensional vectors of observations on the two main eigenvectors ( $\vec{v}_1, \vec{v}_2$ ) obtained with the DA method for the 3-class training set. The three clouds of symbols represent three classes of charge of the example training set:  $Z = 57$  (black circles),  $Z = 56$  (blue squares) and  $Z = 58$  (red triangles).

Having a way to label the classes of the training set and the DA tool to define a low-dimensional space

in which the classes are best separated, one can now project the vectors of observations of unknown class membership onto the optimal reference frame and, using the distributions of the training set, assign to them the most probable (or, if possible, average) labels.

In our application the label (charge) assignment has been done in two ways. Since the beam charge range is quite narrow, we restricted the individual charge identification to 5 classes of charges with  $Z \in [Z_{nom} - 2, Z_{nom} + 2]$  (with nominal charge  $Z_{nom} = 57$  (50) for the nominal  $^{124}\text{La}$  ( $^{107}\text{Sn}$ ) beam) plus two classes with  $Z < Z_{nom} - 2$  and  $Z > Z_{nom} + 2$ , thus altogether 7 classes. In the first approach this definition of classes has been subsequently simplified by splitting the 7 classes into 5 groups, each group containing only 3 classes:  $Z_0$  with  $Z \in [Z_{nom} - 2, Z_{nom} + 2]$ ,  $Z_<$  with  $Z < Z_0$  and  $Z_>$  with  $Z > Z_0$ . This allowed, thanks to the dimensionality reduction of DA, to base the charge assignment on the usage of 2-dimensional histograms, such as the one in Fig. 4, defined using the vectors of the training set.

The other approach was based on the original 7-class definition which lead to a 6-dimensional optimal space after DA. The 6-dimensional distributions of projections of the training vectors were then parametrized assuming their Gaussian shapes and these parametrizations were used for the charge assignment. The first approach, based on the 2-dimensional reference histograms, was found to give about 2% better efficacy of charge recognition as compared to the method based on the Gaussian parametrization.

Fig. 5 shows the proportion of charges reconstructed using the DA method,  $Z_{DA}$ , as a function of the reference charge measured by the MUSIC chamber,  $Z_{MUSIC}$ . The numbers in boxes represent the proportions, in % of the total yield, calculated for the total statistics collected. They are indicated if the contribution exceeds 1%. The sum of the diagonal elements provides the measure of the overall efficacy of the method, *i.e.* the proportion of correctly recognized charges. It amounts to about 86% in case of the nominal " $^{124}\text{La}$ " beam and to about 89% for the " $^{107}\text{Sn}$ " beam. The first and the last bins contain additionally the contributions of all the smaller and greater charges, respectively. In particular, the figure shows that the light impurities formed in reactions on the up-stream material (the first column) amount to about 4-6% of the incoming projectiles. About 50% of them can be properly recognized and eventually rejected dur-

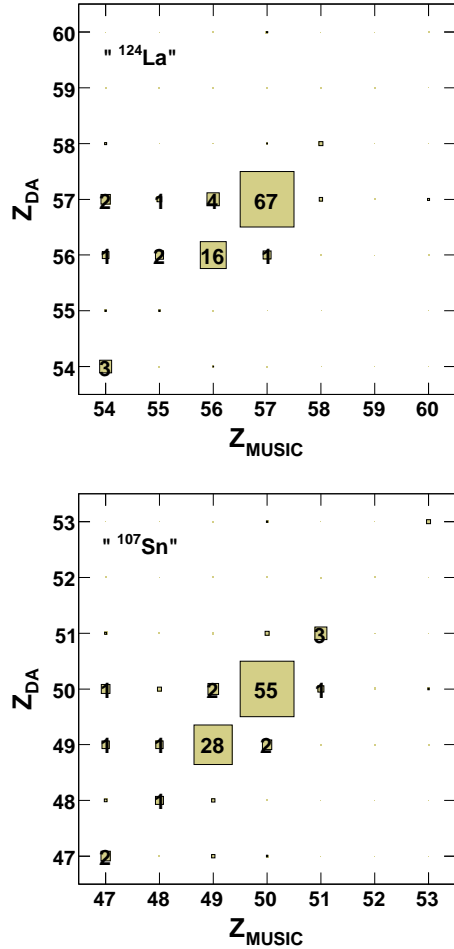


Fig. 5. Contributions of charges reconstructed using the DA-based method ( $Z_{DA}$ ) and the charges measured by the MUSIC chamber ( $Z_{MUSIC}$ ). The numbers in boxes represent the contributions in % of the total yield. The first (last) bin contains also the contributions of all the smaller (greater) charges.

ing the analysis. The methods based on the simple scalar observables have been found to be about 20% less efficacious than the one based on DA.

The ratio of the mass to atomic numbers,  $A/Z$ , of the projectile has been measured with high precision from the time of flight and position at the dispersive focal plane S2 of the FRS. The calibration has been done using the basic equation for identification:

$$B\rho = \frac{A}{Z} \frac{u\beta}{e\sqrt{1-\beta^2}}$$

where,  $B\rho$  is the projectile rigidity and  $A$ ,  $Z$  and  $\beta$  its mass and charge numbers and velocity, respectively;  $u$  and  $e$  are the atomic mass and charge units.

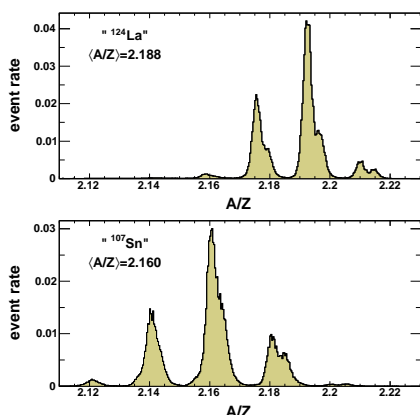


Fig. 6. Distributions of  $A/Z$  for  $^{124}\text{La}$  (top) and  $^{107}\text{Sn}$  (bottom) nominal beams. The numbers in the top left corners specify the average  $\langle A/Z \rangle$  of the secondary beams for the whole experiment.

Figure 6 presents the measured distributions of  $A/Z$  for both secondary beams used in the experiment. The high precision measurement allows to visualize the “fine” structure of the  $A/Z$  groups due to its  $Z$  dependence. The average  $\langle A/Z \rangle$  for the two secondary beams are: 2.188 for the nominal  $^{124}\text{La}$  beam and 2.160 for the  $^{107}\text{Sn}$  beam. The average  $\langle Z \rangle$  for the two beams are 56.8 and 49.7, respectively. The averages take into account variations due to different FRS settings for different groups of runs and are taken over the whole experiment.

Having determined the  $A/Z$  and  $Z$ , the isotopically pure beams can be selected also for events with reacting projectiles. Figure 7 shows the resulting composition of the two secondary beams used in the S254 experiment.

The numbers in the histograms specify the contribution of a given isotope (in %) and are indicated only if the contribution is greater than 1%. Gating on a given atomic and mass number allows to select a 90% pure beam and to also keep away from the light impurities from reactions on the up-stream material.

Summarizing, we have demonstrated a high efficacy of the secondary-beam charge recognition method based on the discriminant analysis technique in an experiment without a dedicated  $Z$ -detector. The method has improved the quality of the S254 experimental data by allowing up to 90% pure isotopic selection of the incoming projectiles.

The authors would like to thank P. Désesquelles for stimulating introduction to DA and valuable comments. This work has been supported by the Polish Ministry of Science and Higher Education

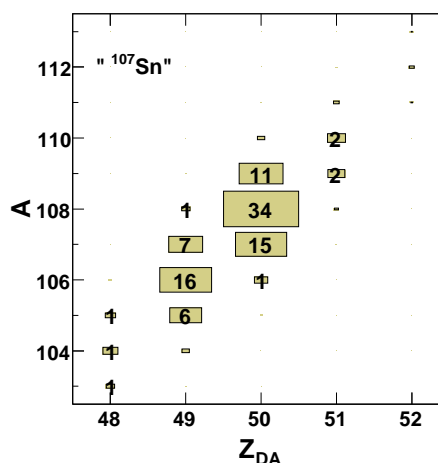
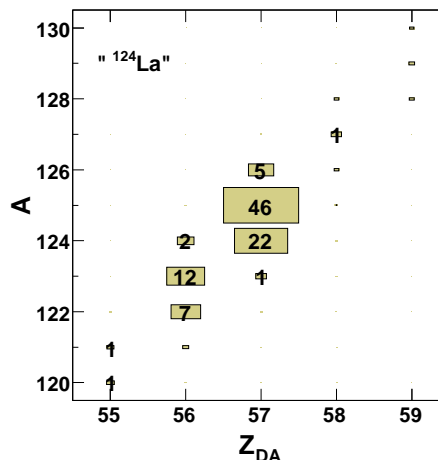


Fig. 7. Mass versus atomic number of the two secondary beams used in the S254 experiment, as obtained from the  $Z$  reconstruction using the DA method and the high precision  $A/Z$  measurement. The numbers in the boxes represent the contribution of a given isotope (in %) to the secondary beam.

under Contracts No. 1 P03B 105 28 (2005 - 2006) and N202 160 32/4308 (2007-2009).

## References

- [1] H. Geissel *et al.*, Nucl. Instr. and Meth. B **70** (1992) 286, <http://www-w2k.gsi.de/frs>
- [2] C. Sienti *et al.*, Nucl. Phys. A **749** (2005) 83c.
- [3] A.K. Jain, R.C. Dubes, “Algorithms for Clustering Data”, Prentice Hall Advanced Reference Series, 1988.
- [4] J. Ye, R. Janardan and Q. Li in “Advances in Neural Information Processing Systems 17”, ed. L.K. Saul, Y. Weiss and L. Bottou, MIT Press, 2005, <http://books.nips.cc/nips17.html>
- [5] P. Désesquelles, Ann. Phys. Fr. **20** (1995) 1.
- [6] R.A. Fisher, Annals of Eugenics, **7** (1936) 179.

[7] P. Désesquelles *et al.*, Phys. Rev. C **62** (2000) 024614.